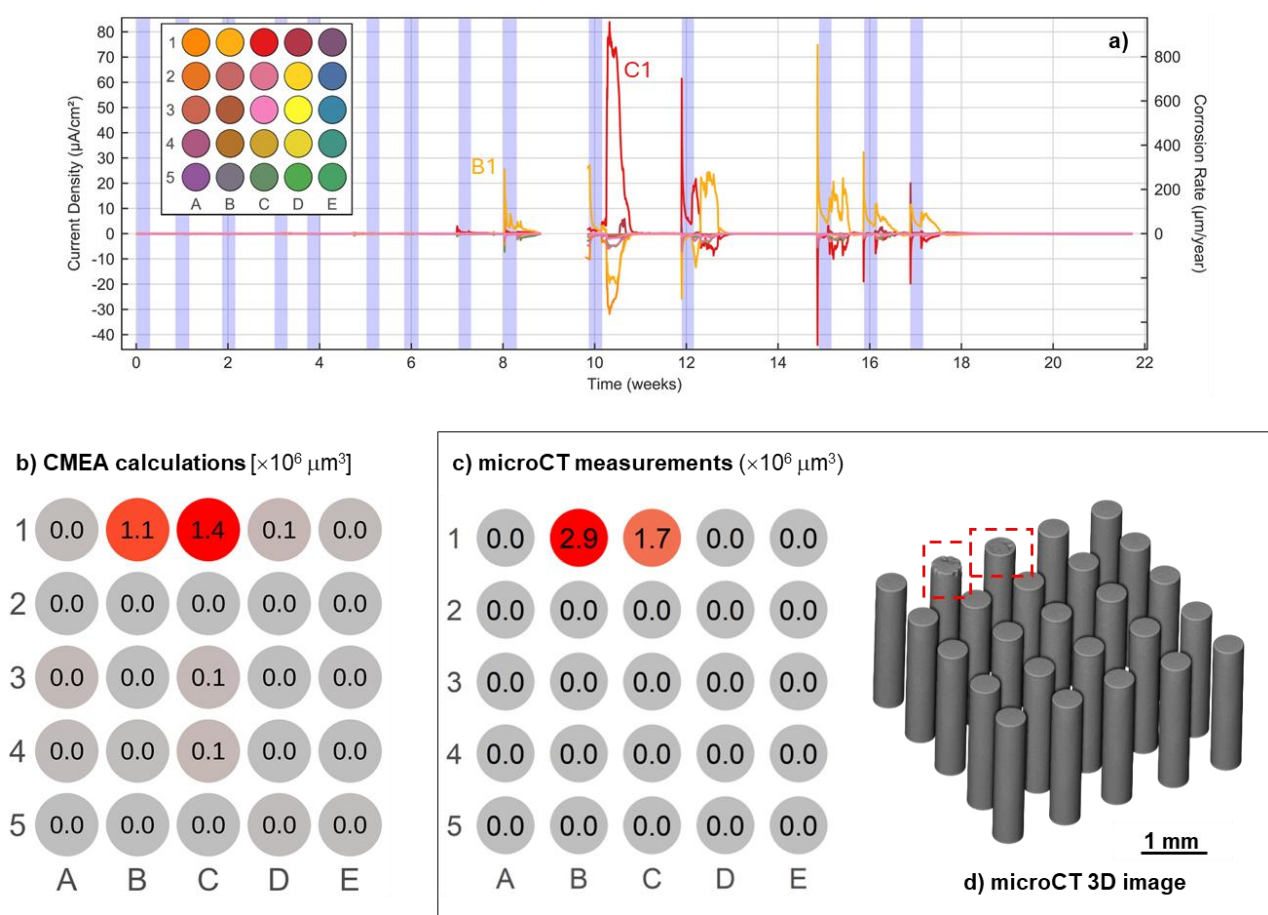
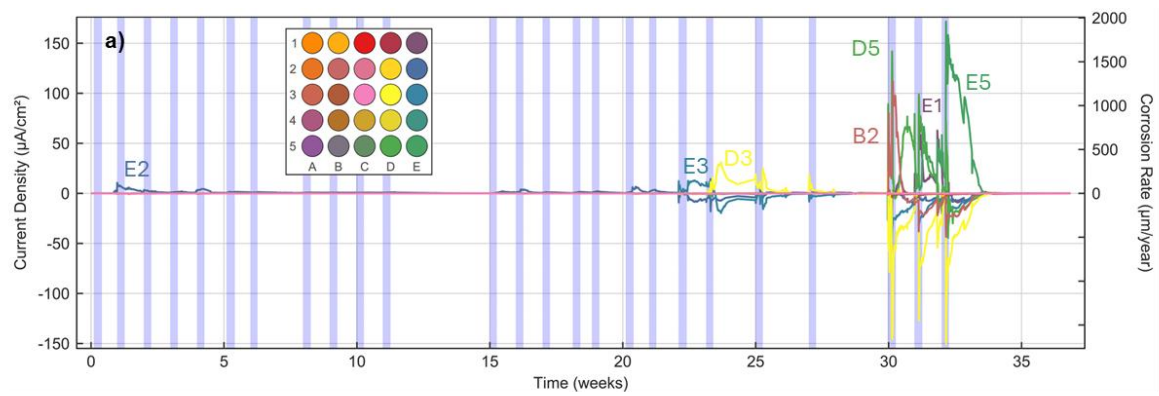


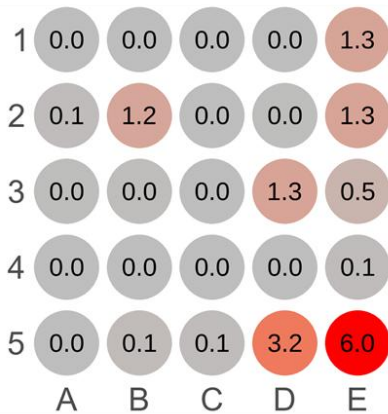
Supplementary material:



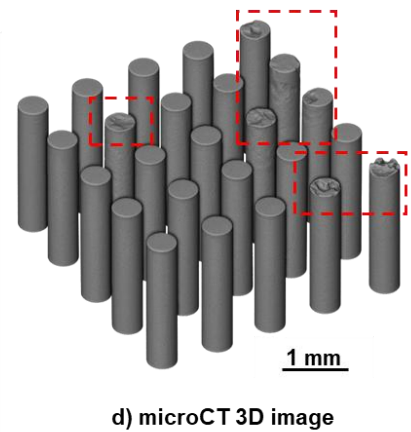
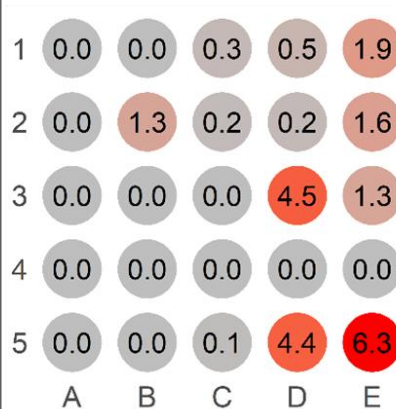
Supplementary Fig. 1. A CMEA sensor embedded in the FA8 (fly ash) alkali-activated mortar: a) continuous measurements of the ANODIC (positive, j_{corr}) and CATHODIC (negative, j_{cath}) current densities (grey sections = wetting, white sections = drying), b) corrosion damage calculated from the measured CMEA anodic currents (D_V), c) corrosion damage measured from the microCT scans, and d) a microCT 3D image of the CMEA following the period of exposure.



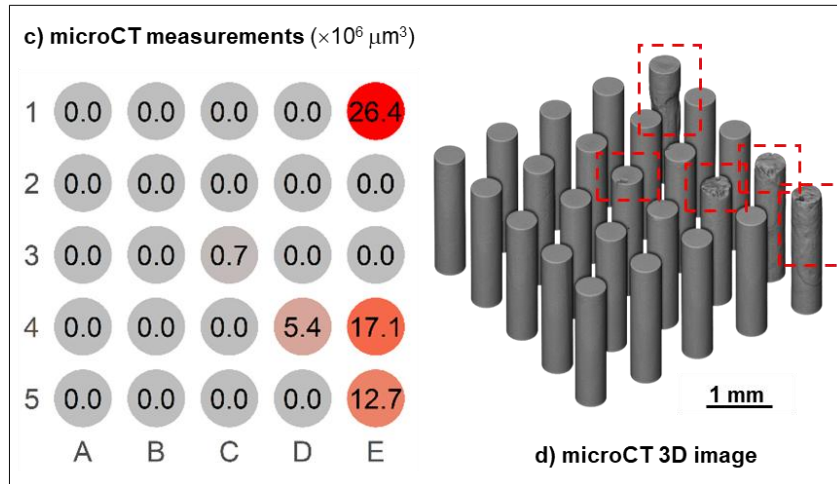
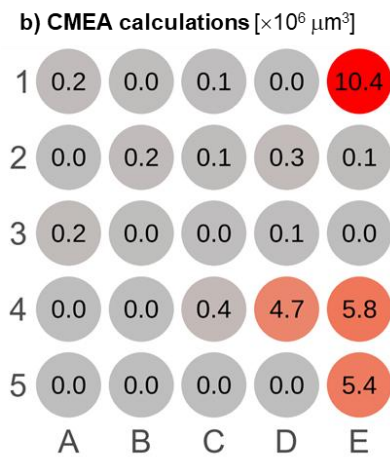
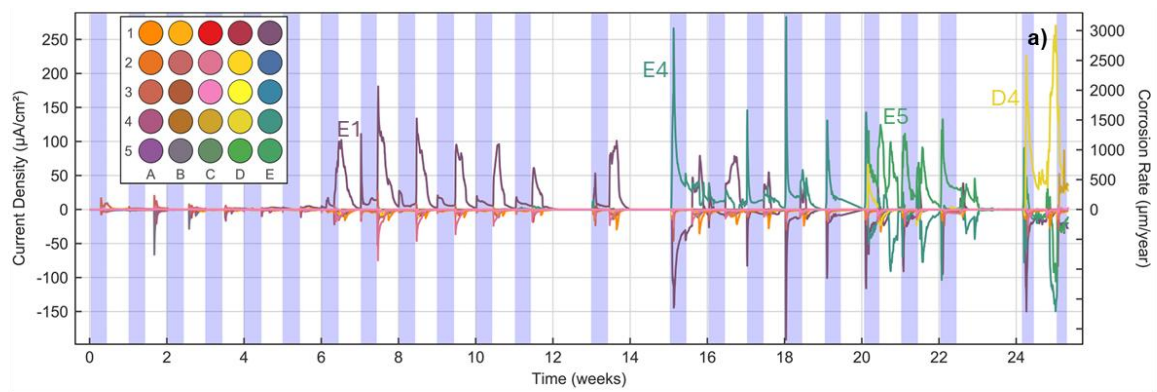
b) CMEA calculations [$\times 10^6 \mu\text{m}^3$]



c) microCT measurements ($\times 10^6 \mu\text{m}^3$)



Supplementary Fig. 2. A CMEA sensor embedded in the MK2 (metakaolin) alkali-activated mortar: a) continuous measurements of the ANODIC (positive, j_{corr}) and CATHODIC (negative, j_{cath}) current densities (grey sections = wetting, white sections = drying), b) corrosion damage calculated from the measured CMEA anodic currents (D_V), c) corrosion damage measured from the microCT scans, and d) a microCT 3D image of the CMEA following the period of exposure.



Supplementary Fig. 3. A CMEA sensor embedded in the S3a-661 (slag) alkali-activated mortar: a) continuous measurements of the ANODIC (positive, j_{corr}) and CATHODIC (negative, j_{cath}) current densities (grey sections = wetting, white sections = drying), b) corrosion damage calculated from the measured CMEA anodic currents (D_V), c) corrosion damage measured from the microCT scans, and d) a microCT 3D image of the CMEA following the period of exposure.